Line-Focus Array Transducers for Effective Actuation of Tissue

Tomotaka Sawada[1], Hideyuki Hasegawa[1,2], and Hiroshi Kanai[2,1*]

[1]*Graduate School of Biomedical Engineering, Tohoku University, Sendai 980-8579, Japan*
[2]*Graduate School of Engineering, Tohoku University, Sendai 980-8579, Japan*

Acoustic radiation forces induced by ultrasound can be used to apply external forces to an object, and the viscoelastic property of the object can be evaluated by measuring the resultant regional displacement of the object using a different ultrasonic probe for measurement. However, according to safety guidelines for the use of ultrasound, the recommended intensity is below $1 \, \text{W/cm}^2$ for continuous waves. Therefore, to generate a measurable displacement or strain by acoustic actuation, a method of effectively applying acoustic radiation forces needs to be devised. A potential way to improve the efficiency of acoustic actuation is to use line-focus transducers. However, there are undesired fluctuations in the emitted sound field due to the finite aperture size with uniform apodization when a single-element line-focus transducer (SELFT) is used to emit plane waves, which are focused only in the elevational direction. To suppress such undesired fluctuations, in the present study, a pair of line-focus array transducers (LFATs) was constructed to realize spatially smoother radiation forces by applying an appropriate apodization. As a result, the three dominant undesired peaks in the sound field emitted from a SELFT were suppressed using the LFATs with the examined appropriate apodization, and the displacement distribution induced in a phantom, which was measured by the phased tracking method using the different ultrasonic probe, became spatially smooth. © 2010 The Japan Society of Applied Physics

1. Introduction

The evaluation of muscle elasticity is important for examining the health of muscle. In this study, acoustic radiation forces resulting from focused continuous ultrasound are simultaneously applied to an object from two opposite horizontal directions and the resultant displacement is measured using another ultrasound transducer.

In recent years, some remote actuation methods based on acoustic radiation forces have been reported. Fatemi and Greenleaf proposed an imaging modality that uses the acoustic responses of an object, which are closely related to the mechanical frequency response of the medium. By measuring the acoustic emission with a hydrophone, hard inclusions such as calcified tissues in soft material were detected experimentally.[1,2] However, the spatial resolution in the depth direction corresponds to the size of the intersectional area of ultrasound beams at two slightly different frequencies and is not particularly high.

Nightingale and coworkers proposed an alternative imaging method in which focused ultrasound is employed to apply a radiation force to soft tissue for a short duration (less than 1 ms). The viscoelastic properties of the tissue were investigated from the magnitude of the transient response, which was measured as the displacement $d(t)$ of the tissue.[3–5] In order to generate a measurable displacement $d(t)$ by several ultrasonic pulses, high-intensity pulsed ultrasound $(1{,}000 \, \text{W/cm}^2)$ was employed. However, according to safety guidelines for the use of ultrasound, the intensity is recommended to be below $240 \, \text{mW/cm}^2$ for pulsed waves and $1 \, \text{W/cm}^2$ for continuous waves.[6] Therefore, the intensity of the pulsed ultrasound employed by Nightingale and coworkers is far greater than that indicated in the safety guidelines.

The maximum intensity of $1 \, \text{W/cm}^2$ for continuous waves given by the safety guidelines corresponds to an acoustic radiation force of $6.67 \, \text{Pa}$, which is very small. Therefore, to generate a measurable displacement by acoustic actuation, a method of effectively applying acoustic radiation forces needs to be devised. In our previous study, we proposed a

method in which two cyclical radiation forces were simultaneously applied to a phantom from two opposite horizontal directions so that the object was cyclically compressed in the horizontal direction.[7] A potential way to further improve the efficiency of acoustic actuation is to use line-focus array transducers (LFATs). In the present study, LFATs were newly constructed, and the voltages applied to the transducer elements were set so that the sound pressure at the focal area became as constant as possible in the lateral direction, whereas the sound field was focused only in the elevational direction. In basic experiments using a phantom, it was confirmed that a more homogeneous distribution of displacements was successfully generated using the dual LFAT compared with that generated by a dual single-element point-focus transducer (SEPFT) or a dual single-element line-focus transducer (SELFT).

2. Principles

2.1 Actuation method using acoustic radiation force

When ultrasound propagates in a medium (density: ρ_1, sound speed: c_1), a constant force is generated in the direction of propagation. This force is called the acoustic radiation force.[8] When an object is assumed to be a perfectly absorbing material, the acoustic radiation pressure, $P_\text{R}(t)$, is defined as the acoustic radiation force per unit area as follows:

$$P_\text{R}(t) = (1 + R^2)e(t), \tag{2.1}$$

where R and $e(t)$ are the pressure reflection coefficient and the energy density at the interface between the medium and the object, respectively. In eq. (2.1), the transmitted wave is assumed to be perfectly absorbed by the object behind the medium. Using the density ρ_2 and sound speed c_2 of the object, the reflection coefficient R and the energy density $e(t)$ are defined by

$$\begin{aligned} R &= \frac{Z_2 - Z_1}{Z_2 + Z_1} \\ &= \frac{\rho_2 c_2 - \rho_1 c_1}{\rho_2 c_2 + \rho_1 c_1}, \end{aligned} \tag{2.2}$$

$$e(t) = \frac{1}{\rho_1 c_1^2} \{p(t)\}^2. \tag{2.3}$$

*E-mail address: kanai@ecei.tohoku.ac.jp

© 2010 The Japan Society of Applied Physics

For example, the speeds of sound in muscle and fat are 1,568 and 1,465 m/s, respectively. By assuming the density of both tissues to be 1.0×10^3 kg/m^3, the reflection coefficient R is 0.034. Thus, R^2 in eq. (2.1) is assumed to be zero.

As shown in eq. (2.3), the energy density $e(t)$ is proportional to the square of the sound pressure $p(t)$ of the incident ultrasonic wave. When two ultrasound waves with the same sound pressure p_0 and slightly different frequencies, f and $f + \Delta f$, are crossed with each other, an acoustic radiation pressure $P_R(t)$, which fluctuates at the frequency difference Δf, is generated in the intersectional area. The sound pressure $p_{sum}(t)$ generated in the intersectional area is given by

$$p_{sum}(t) = p_0 \cos 2\pi f t + p_0 \cos 2\pi (f + \Delta f)t, \quad (2.4)$$

and the resultant energy density $e(t)$ is given by

$$
\begin{aligned}
e(t) &= \frac{1}{\rho_1 c_1^2} [p_{sum}(t)]^2 \\
&= \frac{1}{\rho_1 c_1^2} [p_0 \cos 2\pi f t + p_0 \cos 2\pi (f + \Delta f)t]^2 \\
&= \frac{p_0^2}{\rho_1 c_1^2} \Big[1 + \cos 2\pi \Delta f t + \cos 2\pi (2f + \Delta f)t \\
&\quad + \frac{1}{2} \cos 4\pi f t + \frac{1}{2} \cos 4\pi (f + \Delta f)t \Big].
\end{aligned}
\quad (2.5)
$$

From the second term on the right-hand side of eq. (2.5), it is found that the energy density $e(t)$ has a component at the frequency difference Δf. With respect to the low-frequency component, the acoustic radiation pressure $P_R(t)$ of eq. (2.1) actually acting on the interface is given by

$$
\begin{aligned}
P_R(t) &\simeq (1 + R^2) \frac{p_0^2}{\rho_1 c_1^2} (1 + \cos 2\pi \Delta f t) \\
&\simeq \frac{p_0^2}{\rho_1 c_1^2} (1 + \cos 2\pi \Delta f t).
\end{aligned}
\quad (2.6)
$$

To improve the spatial resolution in the measurement of the response of an object to the acoustic radiation force, an ultrasound correlation-based method, the *phased tracking method*,[9,10] was used to measure the distribution of the minute displacements, $\{d(t)\}$. The accuracy of the displacement measurement by the phased tracking method has already been evaluated to be 0.2 μm by performing basic experiments using a rubber plate.[11]

2.2　Possibility of effective actuation by line-focus transducers

The experimental setup used for actuation and the measurement of resultant displacements is illustrated in Fig. 1. When the elastic modulus of an object is much greater than that of the surrounding medium, a single acoustic radiation force may generate only a change in the position of the object. For the effective generation of strain in the object, we applied two acoustic radiation forces, which were induced by two synchronized ultrasounds both containing frequency components at f and $f + \Delta f$, to two different positions in the object from two opposite directions, as shown in Fig. 1.[7] Therefore, the region compressed by the two acoustic radiation forces was compressed along the horizontal axis.
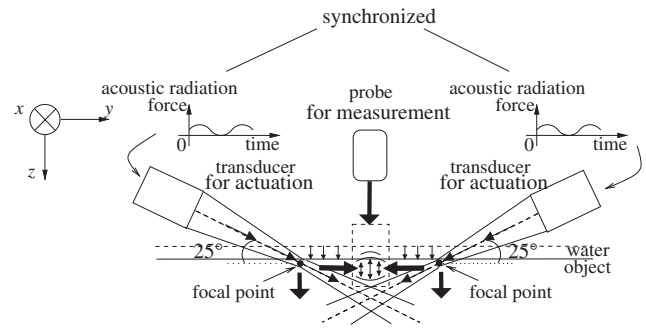

Fig. 1. Illustration of the experimental setup for actuation and the measurement of resultant displacements.
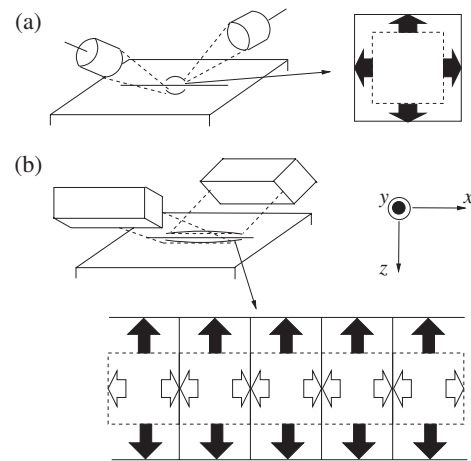

Fig. 2. Illustration of strains generated by (a) the dual point-focus transducer and (b) the dual line-focus transducer.

The directions of the strains generated by a dual point-focus transducer and a dual line-focus transducer are illustrated in Figs. 2(a) and 2(b), respectively. When a region is compressed in the y-direction by two synchronized radiation forces generated by the dual point-focus ultrasonic transducer, as shown in Fig. 2(a), the region expands in both the x- and z-directions owing to its incompressibility. When the dual line-focus ultrasonic transducer is employed, as shown in Fig. 2(b), the region will expand further in the vertical (z) direction than in the case shown in Fig. 2(a) to preserve its volume because the region is difficult to expand in the x direction, as shown in Fig. 2(b), which is theoretically explained as follows:[12]

The strains ε_{pz} and ε_{lz} in the vertical (z) direction generated by the dual point-focus and dual line-focus transducers are respectively given by

$$\varepsilon_{pz} = \frac{\sigma_y}{E} \nu, \quad (2.7)$$

$$\varepsilon_{lz} = \frac{\sigma_y}{E} \nu \cdot (1 + \nu), \quad (2.8)$$

where σ_y, E, and ν are the stress in the y-direction, the Young's modulus, and the Poisson's ratio of an object, respectively. By assuming that the object is an incompressible material ($\nu = 0.5$) such as biological tissue, the strain generated by the dual line-focus transducer illustrated in Fig. 2(b) is $1 + \nu = 1.5$ times larger than that generated by the dual point-focus transducer illustrated in Fig. 2(a).
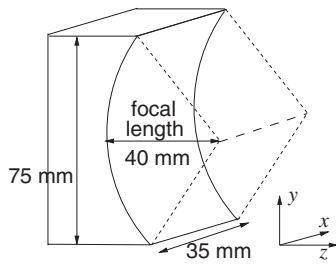
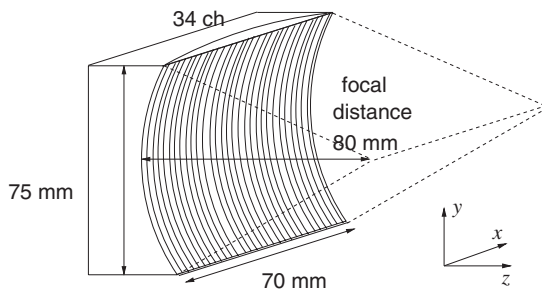**Fig. 3.** Illustration of the SELFT.

Fig. 4. Illustration of the LFAT.

Fig. 5. Illustration of the experimental setup.

In our previous study, a dual SEPFT, whose aperture size and focal distance were both 50 mm, was used for acoustic actuation. In the present study, aiming for effective actuation, a new dual SELFT was constructed as illustrated in Fig. 3. The focal distance was 40 mm. Moreover, a new dual LFAT was also constructed to realize more flexibility in designing the sound fields. The structure of the LFAT is illustrated in Fig. 4. This transducer is composed of 34 elements and, thus, the voltage applied to each element can be controlled. Its aperture in the x-direction is 70 mm wide, which is twice as wide as the SELFT of 35 mm width illustrated in Fig. 3. The element pitch of the LFAT in Fig. 4 is 2.0 mm.

In the present study, the array was divided into three groups: 9 or 3 elements on both sides and 16 or 28 central elements, and the voltages applied to these groups were weighted as ($w_1 : w_2 : w_3$), which was defined as the voltage ratio. The voltages applied to the groups on both sides were set at 20–100% of that applied to the central elements ($w_1, w_3 = 0.2$–1.0, $w_2 = 1.0$).

3. Experimental Setup

Basic experiments using a phantom were conducted to confirm whether it was homogeneously actuated along the focal region of each transducer by measuring the spatial distribution of the displacements $\{d_z(x, z)\}$ in the vertical (z) direction at multiple points $\{x, z\}$ in the phantom.

The experimental setup is illustrated in Fig. 5. In order to measure the displacement distribution $\{d_z(x, z)\}$ at a high spatial resolution, we employed ultrasonic diagnostic equipment (Dynamic Imaging DIASUS) with a linear-type probe (center frequency: 16 MHz). The equipment was modified to detect the minute displacement of an object by the ultrasonic phased tracking method.[9,10] The sound pressure of the ultrasonic pulse used for measurement is
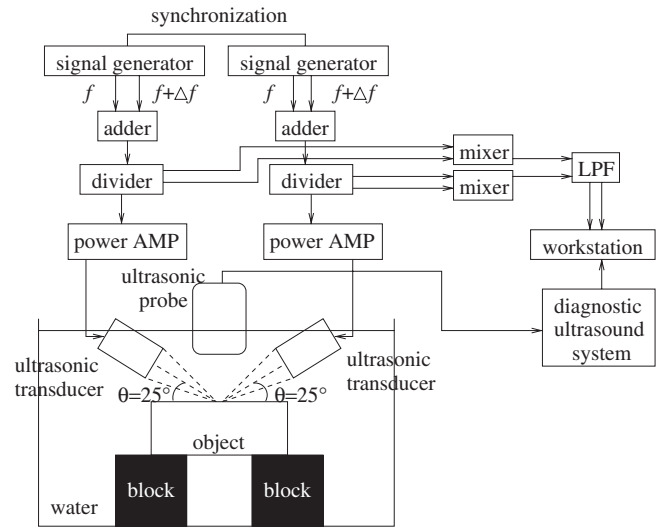
56 kPa, which corresponds to an acoustic radiation force of one-quarter that produced by the ultrasound used for actuation. In addition, the ultrasonic pulses used for measurement are transmitted at a pulse repetition frequency of 15 kHz, which is much larger than the frequency (5 Hz) of cyclic fluctuation of the radiation force produced by the ultrasound used for actuation. Therefore, the radiation forces produced by the ultrasonic pulses used for measurement hardly affect that produced by the ultrasound used for actuation.

A homogeneous object made of gel ($60 \times 60 \times 25$ mm^3, containing 5% carbon powder by weight to provide sufficient scattering) was placed in a water tank as shown in Fig. 5. To apply the radiation pressures $P_{R1}(t)$ and $P_{R2}(t)$, a dual ultrasonic transducer was employed. Each ultrasonic transducer (center frequency: 1 MHz) was driven by the sum of continuous waves at two slightly different frequencies of 1 MHz and 1 MHz + 5 Hz. Each focal point was set at the surface of the object at a beam angle of 25 degrees from the horizontal direction.

The ultrasound signals used for actuation (approximately 1 MHz) unintentionally received by the linear-array probe (16 MHz) used for measurement were removed by filtering to make it possible to estimate the displacement distribution $\{d_z(x, z)\}$.

4. Results

### 4.1 Measurement of displacement at the boundary between oil and water

As illustrated in Fig. 6, the displacement distribution $\{d_z(x, z)\}$ along the interface between oil and water was measured with ultrasound since the interface between liquids is easily actuated at a large amplitude and the actuated region can be easily identified. In this experiment, both beam angles of the dual ultrasound wave used for actuation were set at 25°.

Figures 7(a) and 7(b) show the spatial distributions $\{d_z(x, z)\}$ of displacements during one cycle of acoustic radiation forces generated by the dual SEPFT and the dual SELFT, respectively. Blue and red correspond to the upward and downward displacements, respectively. Using the dual
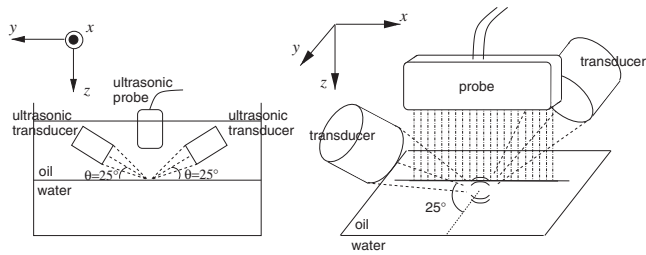
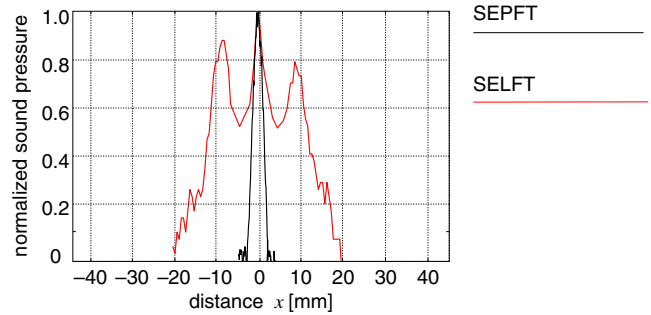**Fig. 6.** Illustration of the displacement measurement at the boundary of oil and water.
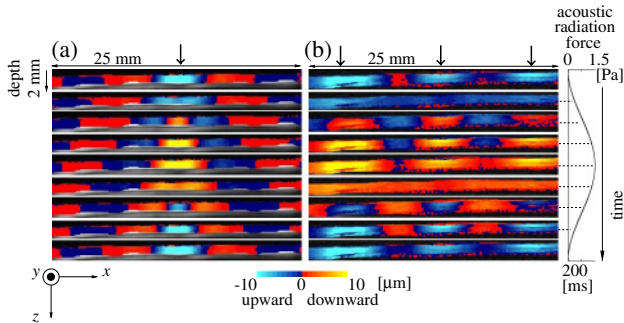
Fig. 7. (Color online) Spatial distributions of the displacements $\{d_z(x,z)\}$ of the interface between oil and water generated by (a) the dual SEPFT and (b) the dual SELFT.

Fig. 8. (Color online) Spatial distributions of the sound pressure along the *x*-axis at the focal distances measured for the SEPFT and the SELFT.

Fig. 9. Illustration of simulation method for calculating the spatial distributions of the sound pressure along the *x*-axis at the focal distances.

SEPFT, the generated displacements $\{d_z(x,z)\}$ were large only at the focal point of the dual transducer [the center in the lateral (*x*) direction]. The purpose of using the dual SELFT was to actuate a wider region in an object almost uniformly in the horizontal (*x*) direction. However, in Fig. 7(b), there were three regions where the amplitudes of the displacements, $\{d_z(x,z)\}$, were large, as shown by the downward arrows in Fig. 7(b).
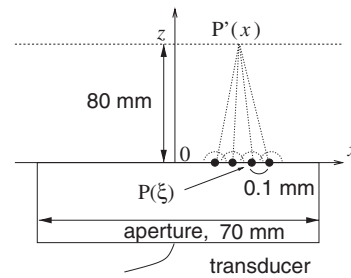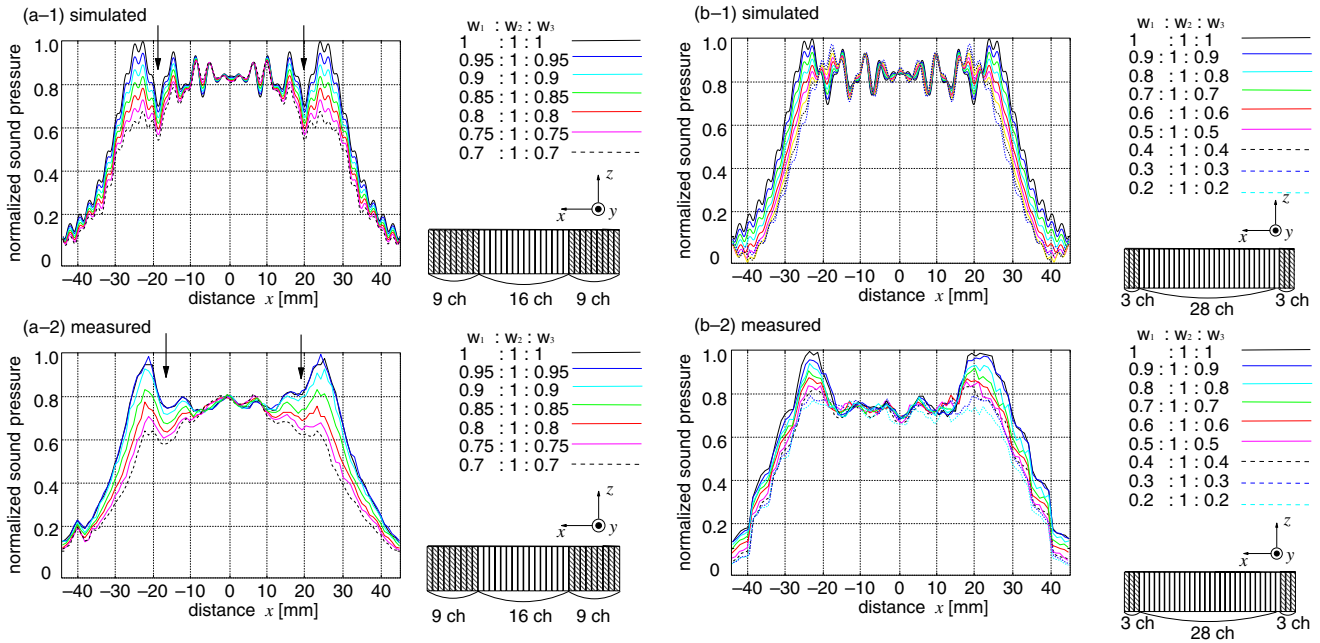
Figure 8 shows the spatial distributions of the sound pressure in the *x*-direction at the focal distances of the SEPFT ($z = 50$ mm) and the SELFT ($z = 40$ mm). As shown by the red line in Fig. 8, there were three peaks in the sound pressure distribution generated by the SELFT owing to the finite size of the aperture.[13]

4.2 Revised sound field using the LFAT

To obtain a flat distribution of sound pressure, the array was divided into three groups, $\{i\}$ ($i = 1, 2, 3$), and the voltages applied to these groups were weighted as ($w_1 : w_2 : w_3$). The number of elements in each group and the weight of the voltage applied to each group were determined by simulation of the sound field at the focal distance of the LFAT. In this simulation, as shown in Fig. 9, the aperture of the transducer was assumed to be an assembly of point sound sources. The wavelength λ, the aperture size L of the transducer, and the pitch Δx between the point sound sources were set at 1.5, 70, and 0.1 mm, respectively. The *y*-direction (elevational direction) is not considered in this simulation because it mainly changes the amplitude of the sound field produced at the focal distance. The number of elements n_i of each group i was varied between ($n_1 = n_3 = 16$ ch, $n_2 = 2$ ch) and ($n_1 = n_3 = 1$ ch, $n_2 = 32$ ch). Two examples are shown below.

Figures 10(a-1) and 10(a-2) show the first example (pattern A) of the simulated and measured spatial distributions of sound pressures in the *x*-direction at a focal distance of 80 mm under various voltage ratios ($w_1 : w_2 : w_3$) for the three groups (9 ch : 16 ch : 9 ch) of the LFAT. When the voltages applied to the 9 elements (groups 1 and 3) on both sides were equal to the voltage applied to the 16 central elements ($w_1 = w_2 = w_3 = 1.0$), the sound pressures on both sides were significantly larger than that at the center. The peaks in the sound pressure decreased as the voltage applied to the groups on both sides decreased and, at $w_1 = w_3 = 0.85$ ($w_2 = 1.0$), the sound pressures on both sides became similar to that at the center.

Similarly, Figs. 10(b-1) and 10(b-2) show the calculated and measured spatial distributions of sound pressures in the *x*-direction under various voltage ratios ($w_1 : w_2 : w_3$) for the three groups (3 ch : 28 ch : 3 ch), defined as pattern B. In this case, at $w_1 = w_3 = 0.3$ ($w_2 = 1.0$), the sound pressures on both sides became similar to that at the center.

Figure 11 shows the spatial distributions of the sound pressures generated by the SELPT, the SELFT, and the LFAT with a voltage ratio of $w_1 = w_3 = 0.85$ (9 elements on each side) and $w_2 = 1.0$ (16 central elements) in the case of pattern A and with a voltage ratio of $w_1 = w_3 = 0.3$ (3 elements on each side) and $w_2 = 1.0$ (28 central elements) in the case of pattern B. A wider and smoother spatial distribution of the sound pressure was successfully realized by the LFAT. Additionally, pattern B realized a flatter distribution than pattern A. As shown in Fig. 10, when the voltages applied to the groups on both sides decreased, in the case of pattern A, sound pressures in broader regions on both sides were decreased compared with pattern B. As a result, for pattern A, large dips were generated slightly

Fig. 10. (Color online) Calculated and measured spatial distributions of the sound pressure along the *x*-axis at the focal distance of the LFAT. The voltages applied to the three groups [(a) 9 ch : 16 ch : 9 ch, (b) 3 ch : 28 ch : 3 ch] of the transducer elements were weighted.
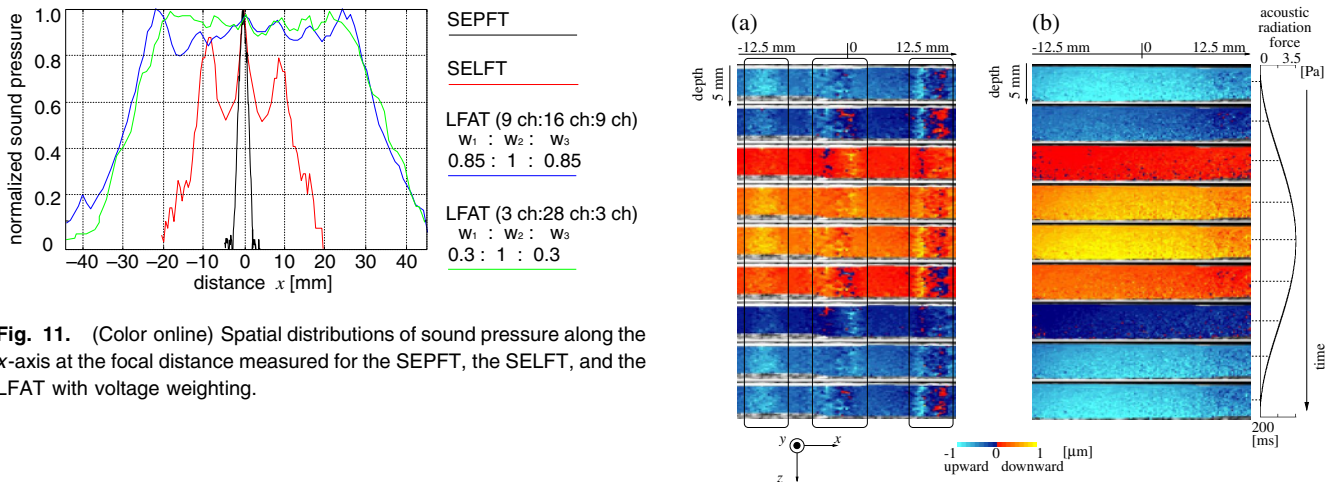
Fig. 11. (Color online) Spatial distributions of sound pressure along the *x*-axis at the focal distance measured for the SEPFT, the SELFT, and the LFAT with voltage weighting.
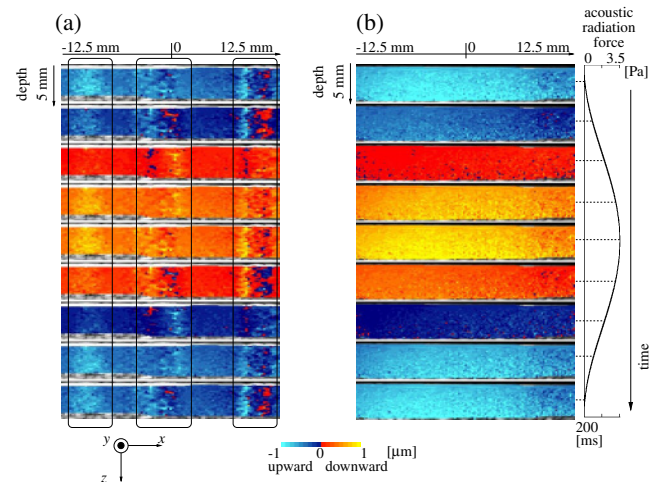
Fig. 12. (Color online) Spatial distributions of displacements $\{d_z(x,z)\}$ in a phantom generated by (a) the dual SELFT and (b) the dual LFAT.

inside of the peaks on both sides as shown by the arrows in Fig. 10. On the other hand, for pattern B, a decrease in the applied voltage had little effect on these regions. From these simulations, it was determined that pattern B was more suitable for realizing a flat distribution of sound pressure.

4.3 Measurement of displacements in a phantom

Figures 12(a) and 12(b) show the spatial distributions of displacements $\{d_z(x,z)\}$ during one cycle of the acoustic radiation forces generated by the dual SELFT and the dual LFAT at $w_1 = w_3 = 0.3$ ($w_2 = 1.0$) for the three groups (3 ch : 28 ch : 3 ch), respectively. Blue and red correspond to the upward and downward displacements at amplitudes of up to 1 μm, respectively. Overall downward displacements were generated by the downward component of acoustic radiation forces during the period when the acoustic radiation forces increased as shown in Fig. 1. As shown in Fig. 12(a), the spatial distribution of displacements, $\{d_z(x,z)\}$, generated by the dual SELFT was nonuniform since the displacements in the black boxes were significantly larger than those elsewhere. On the other hand, as shown in Fig. 12(b), the spatial

distribution of displacements, $\{d_z(x,z)\}$, generated by the dual LFAT is more uniform during a cycle of the acoustic radiation forces.

5. Discussion

In this study, in basic experiments using a phantom, it was confirmed that a more homogeneous distribution of displacements was generated using the dual LFAT than using the dual SEPFT or the dual SELFT. To show the improvement in the effectiveness of actuation using the dual LFAT, it is necessary to measure the strain generated by the ultrasonic actuation. However, in the present study, it was difficult to generate a measurable strain owing to the limitations of the hardware employed for the ultrasound transmission. The maximum sound pressure that could be generated in the present study by the dual LFAT was

100 kPa, which corresponds to 0.225 W/cm^2. In a future work, we plan to increase the acoustic output to close to 1 W/cm^2 by improving the hardware to generate a measurable strain and to show that the effectiveness of the actuation is improved using the LFAT.

6. Conclusions

In this study, for effective ultrasonic actuation, we improved ultrasonic fields using a dual LFAT. A more desirable flat distribution of the sound pressure compared with that generated by a dual SELFT was obtained, and the displacements in a phantom generated by the dual LFAT at amplitudes of 1 μm were almost uniform.

1) M. Fatemi, L. E. Wold, A. Alizod, and J. F. Greenleaf: IEEE Trans. Med. Imaging **21** (2002) 1.
2) M. Fatemi and J. F. Greenleaf: Proc. Natl. Acad. Sci. U.S.A. **96** (1999) 6603.
3) K. Nightingale, M. S. Soo, R. Nightingale, and G. Trahey: Ultrasound Med. Biol. **28** (2002) 227.
4) G. E. Trahey, M. L. Palmeri, R. C. Bentley, and K. R. Nightingale: Ultrasound Med. Biol. **30** (2004) 1163.
5) B. J. Fahey, K. R. Nightingale, R. C. Nelson, M. L. Palmeri, and G. E. Trahey: Ultrasound Med. Biol. **31** (2005) 1185.
6) Japan Society of Ultrasonics in Medicine: Cho-onpa Igaku **11** (1984) 41 [in Japanese].
7) H. Hasegawa, M. Takahashi, Y. Nishio, and H. Kanai: Jpn. J. Appl. Phys. **45** (2006) 4706.
8) G. R. Torr: Am. J. Phys. **52** (1984) 402.
9) H. Kanai, M. Sato, Y. Koiwa, and N. Chubachi: IEEE Trans. Ultrason. Ferroelectr. Freq. Control **43** (1996) 791.
10) H. Kanai, H. Hasegawa, N. Chubachi, Y. Koiwa, and M. Tanaka: IEEE Trans. Ultrason. Ferroelectr. Freq. Control **44** (1997) 752.
11) H. Kanai, K. Sugimura, Y. Koiwa, and Y. Tsukahara: Electron. Lett. **35** (1999) 949.
12) A. E. H. Love: *A Treatise on the Mathematical Theory of Elasticity* (Cambridge University Press, New York, 1952).
13) G. S. Kino: *Acoustic Waves* (Prentice Hall, New York, 1987).
14) Y. Odagiri, H. Hasegawa, and H. Kanai: Jpn. J. Appl. Phys. **47** (2008) 4193.